





Ethanol Metabolism Dynamics in *Clostridium ljungdahlii* Grown on Carbon Monoxide

Zi-Yong Liu,^a De-Chen Jia,^b Kun-Di Zhang,^c Hai-Feng Zhu,^a Quan Zhang,^d Wei-Hong Jiang,^b  Yang Gu,^b  Fu-Li Li^a

^aShandong Provincial Key Laboratory of Synthetic Biology, Key Laboratory of Biofuels, Qingdao Institute of Bioenergy and Bioprocess Technology, Chinese Academy of Sciences, Qingdao, People's Republic of China

^bKey Laboratory of Synthetic Biology, CAS Center for Excellence in Molecular Plant Sciences, Shanghai Institute of Plant Physiology and Ecology, Chinese Academy of Sciences, Shanghai, People's Republic of China

^cState Key Laboratory of Microbial Technology, Shandong University, Qingdao, People's Republic of China

^dSinopec Dalian (Fushun) Research Institute of Petroleum and Petrochemicals, Dalian, People's Republic of China

ABSTRACT Bioethanol production from syngas using acetogenic bacteria has attracted considerable attention in recent years. However, low ethanol yield is the biggest challenge that prevents the commercialization of syngas fermentation into biofuels using microbial catalysts. The present study demonstrated that ethanol metabolism plays an important role in recycling NADH/NAD⁺ during autotrophic growth. Deletion of bifunctional aldehyde/alcohol dehydrogenase (*adhE*) genes leads to significant growth deficiencies in gas fermentation. Using specific fermentation technology in which the gas pressure and pH were constantly controlled at 0.1 MPa and 6.0, respectively, we revealed that ethanol was formed during the exponential phase, closely accompanied by biomass production. Then, ethanol was oxidized to acetate via the aldehyde ferredoxin oxidoreductase pathway in *Clostridium ljungdahlii*. A metabolic experiment using ¹³C-labeled ethanol and acetate, redox balance analysis, and comparative transcriptomic analysis demonstrated that ethanol production and reuse shared the metabolic pathway but occurred at different growth phases.

IMPORTANCE Ethanol production from carbon monoxide (CO) as a carbon and energy source by *Clostridium ljungdahlii* and "*Clostridium autoethanogenum*" is currently being commercialized. During gas fermentation, ethanol synthesis is NADH-dependent. However, ethanol oxidation and its regulatory mechanism remain incompletely understood. Energy metabolism analysis demonstrated that reduced ferredoxin is the sole source of NADH formation by the Rnf-ATPase system, which provides ATP for cell growth during CO fermentation. Therefore, ethanol production is tightly linked to biomass production (ATP production). Clarification of the mechanism of ethanol oxidation and biosynthesis can provide an important reference for generating high-ethanol-yield strains of *C. ljungdahlii* in the future.

KEYWORDS CO fermentation, *Clostridium ljungdahlii*, acetate, acetogenesis, ethanol oxidation

Ethanol, an important chemical and cost-effective product, has widespread applications in the industrial and medical fields (1). Traditionally, bioethanol is produced from starch via microbial fermentation. Considering the rapid growth of the global population and the demand for food, lignocellulosic biomass can instead be utilized for producing bioethanol, known as a second-generation ethanol fuel. However, a pretreatment step and usage of an expensive exogenous hydrolytic enzyme are required to obtain soluble sugars before microbial fermentation, making the entire process less cost-effective (2). In this regard, syngas from biomass gasification is another satisfactory

Citation Liu Z-Y, Jia D-C, Zhang K-D, Zhu H-F, Zhang Q, Jiang W-H, Gu Y, Li F-L. 2020. Ethanol metabolism dynamics in *Clostridium ljungdahlii* grown on carbon monoxide. *Appl Environ Microbiol* 86:e00730-20. <https://doi.org/10.1128/AEM.00730-20>.

Editor M. Julia Pettinari, University of Buenos Aires

Copyright © 2020 American Society for Microbiology. All Rights Reserved.

Address correspondence to Yang Gu, Ygu02@sibs.ac.cn, or Fu-Li Li, lifl@qibebt.ac.cn.

Received 26 March 2020

Accepted 11 May 2020

Accepted manuscript posted online 15 May 2020

Published 2 July 2020

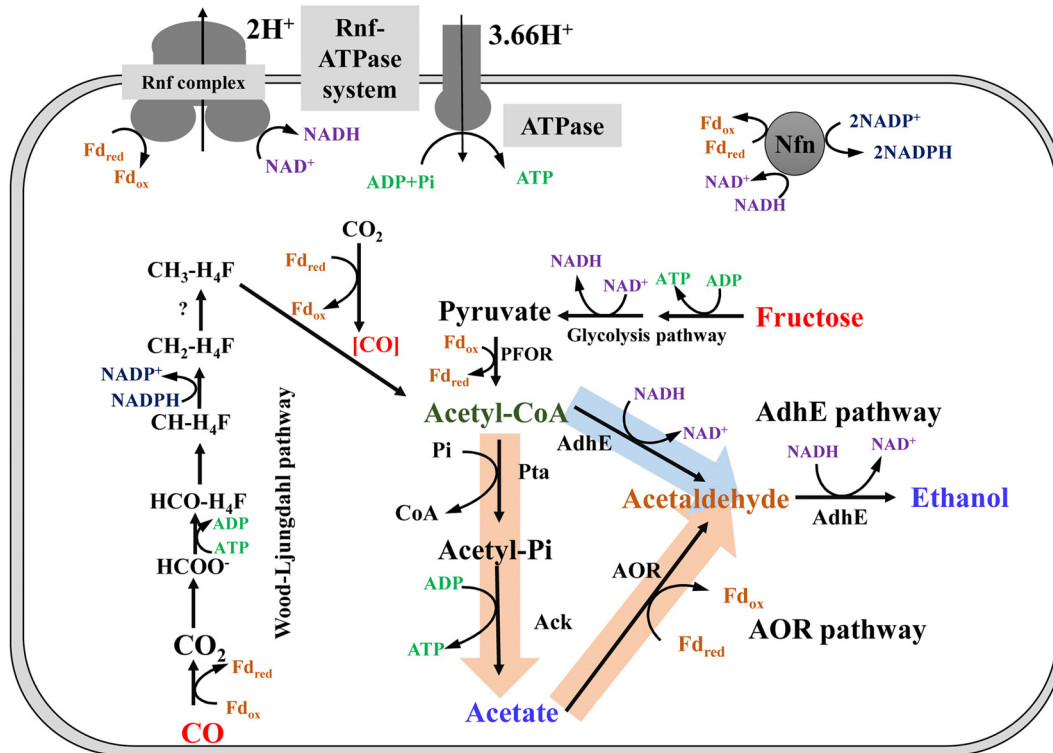


FIG 1 Metabolic pathway of ethanol biosynthesis in *C. ljungdahlii*. Abbreviations used: Pta, *pta*, phosphotransacetylase; Ack, *ack*, acetate kinase; AdhE, *adhE*, aldehyde/alcohol dehydrogenase; AOR, *aor*, acetaldehyde:ferredoxin oxidoreductase; PFOR, *pfor*, pyruvate:ferredoxin oxidoreductase; LdhA, *ldhA*, lactate dehydrogenase; ALDC, *aldc*, acetolactate decarboxylase; 23BDH, *bdh*, 2,3-butanediol dehydrogenase; Fd_{red}, reduced ferredoxin; Fd_{ox}, oxidized ferredoxin; Nfn, electron-bifurcating and ferredoxin-dependent transhydrogenase; Rnf complex, membrane-associated and energy-conserving reduced ferredoxin: NAD⁺ oxidoreductase. The Rnf-ATPase system is a system of two enzyme complexes in which the Rnf complex generates a proton gradient across the membrane by the oxidation of Fd_{red} with NAD⁺. The second enzyme complex, the ATPase complex, consumes the proton gradient and phosphorylates ADP to ATP in the cytoplasm. AdhE pathway, ethanol formation by AdhE catalysis; AOR pathway, AOR participates in acetate and ethanol formation.

feedstock for ethanol production by *Clostridium ljungdahlii*, "*Clostridium autoethanogenum*," and *Clostridium carboxidivorans* (3–13).

C. ljungdahlii and *C. autoethanogenum* were originally described as separate species; however, comparison of their genomic sequences has indicated that they belong to the same species (4, 14). These microorganisms can use carbon monoxide (CO) as a carbon and energy source for ethanol production (7, 11, 13). Two ethanol biosynthesis pathways have been reported (Fig. 1) (15). One is the classic ethanol formation pathway, starting with acetyl-CoA as the precursor, which is converted to ethanol by two redox reactions involving two bifunctional aldehyde/alcohol dehydrogenases encoded by two *adhE* genes. This pathway is named the AdhE pathway. In the other pathway, named the AOR pathway, acetate acts as a precursor, and acetaldehyde:ferredoxin oxidoreductase encoded by *aor* catalyzes the redox reaction of acetaldehyde formation (15). Ethanol synthesis from acetaldehyde overlaps in the two ethanol formation pathways. Deleting *adhE1/2* significantly inhibits ethanol production during heterotrophic fermentation by *C. ljungdahlii* (16). Therefore, AdhE is important for ethanol formation (13, 15–17). Acetate supplementation and deletion of *aor1* and *aor2* in experiments with *C. autoethanogenum* using CO as the carbon source has revealed that the AOR pathway plays a critical role in the conversion of acids to alcohols. Interestingly, inactivation of *aor2* alone elevates ethanol production under the same cultivation conditions (15). Taken together, although important aspects of ethanol production have been elucidated, little is known regarding the regulatory mechanisms of ethanol production in these organisms (18–21).

During acetaldehyde synthesis, the AOR pathway requires reduced ferredoxin

TABLE 1 Enzyme activity assay at 48 h and the final product titers of *C. ljungdahlii* WT, $\Delta adhE1$ mutant, and $\Delta adhE1 \Delta adhE2$ mutant strains in YTF and modified DSMZ 879 medium

Strain	YTF medium				Modified DSMZ 879 medium	
	AdhE (U/mg)	AOR (U/mg)	Ethanol (mM)	Acetate (mM)	Ethanol (mM)	Acetate (mM)
Wild type	0.07	0.1	48 ± 2	83 ± 13	17 ± 0.7	37 ± 2
$\Delta adhE1$ mutant	<0.01	0.01	61 ± 4	62 ± 1	27 ± 0.8	29 ± 0.1
$\Delta adhE1 \Delta adhE2$ mutant	<0.01	<0.01	22 ± 2	84 ± 1	ND ^a	39 ± 4

^aND, not detectable.

(Fd_{red}) as a cofactor, whereas the AdhE pathway requires NADH (Fig. 1). Thus, ethanol biosynthesis is dependent on energy metabolism in *C. ljungdahlii* and *C. autoethanogenum*. In autotrophic microbes growing on CO, Fd_{red} produced via CO oxidization is the primary energy source. ATP, NADH, and NADPH are generated via oxidation of Fd_{red} (17, 18, 22). Among these energy equivalents, ATP can also be generated by substrate-level phosphorylation through acetate formation. Considering ATP consumption by formyl-THF formation in the Wood-Ljungdahl pathway (WLP), there is no net ATP production by substrate-level phosphorylation during gas fermentation. Therefore, ATP is mainly generated by membrane-bound ATP synthase and a transmembrane proton (H^+) gradient, which is established via an oxidation reaction of Fd_{red} with Rnf complex (21, 23–27). On the other hand, NADH is generated as an electron acceptor. It must be coupled with another redox reaction to maintain the redox balance in cells. One of the main outlets for this is ethanol biosynthesis, which requires NADH as an electron donor during autotrophic growth (18, 28, 29). Although the detailed energy metabolic net is unclear for gas fermentation in *C. ljungdahlii* and *C. autoethanogenum*, it is obvious that ethanol formation is tightly associated with energy conservation, especially ATP generation (20).

In this work, *adhE* genes of *C. ljungdahlii* were deleted using CRISPR-Cas9 technology to eliminate the ethanol synthesis pathway. The gene deletion mutants and wild type (WT) were cultured in the presence of CO to elucidate the ethanol formation pathway in *C. ljungdahlii* grown autotrophically. The ethanol production dynamics were investigated and the regulatory mechanisms were analyzed.

RESULTS AND DISCUSSION

Deletion of *adhE* genes. In *C. ljungdahlii*, ethanol synthesis is NADH-dependent, and AdhE is critical for both the AdhE and AOR pathways (Fig. 1). Two *adhE* genes (*adhE1* [CLJU_c16510] and *adhE2* [CLJU_c16520]) encoding AdhE enzymes were found in the genome of *C. ljungdahlii* (13). A CRISPR-Cas9-based genome editing system (30) was used to delete *adhE* genes, generating a $\Delta adhE1$ mutant and a double deletion mutant, the $\Delta adhE1 \Delta adhE2$ mutant (i.e., the $\Delta adhE1+2$ mutant). The $\Delta adhE1$ mutant was described previously (30) and was used as the parental strain to generate the double mutant in this work. Genomic DNA of putative double mutants in selective plates was extracted, and then DNA fragments were PCR-amplified using the primers *adhE1-f/adhE2-r*. Positive bands were obtained and sequenced to confirm the deletion of *adhE1* and *adhE2* (see Fig. S1 in the supplemental material).

Batch fermentation of *adhE* deletion mutants of *C. ljungdahlii* on fructose. During growth on fructose in yeast extract-tryptone-fructose (YTF) medium, two mutants ($\Delta adhE1$ and the $\Delta adhE1 \Delta adhE2$ mutant) eventually achieved a similar cell density that was 76% lower than the WT, suggesting that *adhE* knockout affects cell energy metabolism (Fig. S2). In terms of the primary end products, the $\Delta adhE1 \Delta adhE2$ mutant produced 54% less ethanol (22 ± 2 mM) than the WT (48 ± 2 mM) (Table 1), which is in agreement with previous results obtained by Leang et al. (16). The $\Delta adhE1$ mutant produced 30% less ethanol than the WT (30); however, after three sequential subcultures, this mutant restored its ability to produce ethanol and even generated 27% higher titers of ethanol (61 ± 4 mM) than the WT in this study (Table 1). The details of the mechanism of this phenomenon need further investigation. To further test the

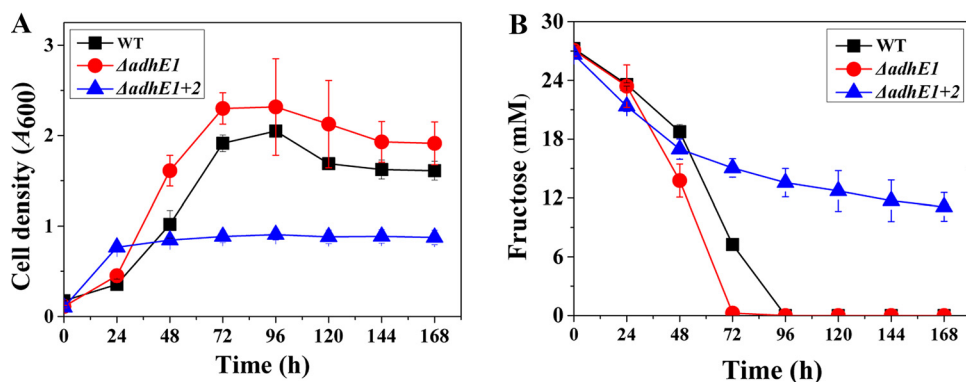


FIG 2 Growth and fructose uptake profiles of *C. ljungdahlii* WT (black squares), $\Delta adhE1$ mutant (red circles) and $\Delta adhE1 \Delta adhE2$ mutant (blue triangles) strains grown on defined DSMZ 879 medium. (A) Growth profiles. (B) Fructose residue.

impact of *adhE* deletion, specific activities of AdhE and AOR were determined in the cell extracts of the WT and *adhE* deletion mutant strains collected at 48 h (Table 1). Trace-specific activities of AdhE were observed in the $\Delta adhE1$ and $\Delta adhE1 \Delta adhE2$ mutants, indicating that *adhE1* is the dominant functional gene during the catalysis reaction from acetaldehyde to ethanol. The specific activity of AdhE in the WT was 0.07 U/mg, exceeding the values for *adhE* mutants (Table 1). Concerning the specific activity of AOR, the value for the WT was 0.1 U/mg, which was much higher than that of the $\Delta adhE1$ (0.01 U/mg) and $\Delta adhE1 \Delta adhE2$ mutants (0.007 U/mg) (Table 1). Analyses of these enzyme activities indicated that *adhE* deletions significantly decreased both AdhE and AOR activities in the mutants.

YTF medium, containing tryptone and yeast extract, is a nutrient-rich medium which possibly affects growth and ethanol formation during fermentation. Thus, a chemically defined medium (modified DSMZ 879 medium) was used to culture the WT and the *adhE* mutants. The growth and fermentation profiles of the WT and the $\Delta adhE1$ strain were similar (Fig. 2, Fig. S3). The $\Delta adhE1$ strain generated 59% higher ethanol titers (27 ± 0.8 mM) than the WT (17 ± 0.7 mM) (Table 1). Compared with the finding for the WT, the $\Delta adhE1 \Delta adhE2$ mutant displayed diminished growth and consumed less fructose during fermentation. In total, 11 ± 1.5 mM fructose was detected in the broth of the $\Delta adhE1 \Delta adhE2$ mutant, whereas the WT and $\Delta adhE1$ strains completely exhausted fructose before 96 h of culture. Furthermore, ethanol was not detected in the broth for the $\Delta adhE1 \Delta adhE2$ mutant, indicating that deletion of two *adhE* genes eliminates ethanol biosynthesis completely.

C. ljungdahlii possesses two adjacent *adhE* genes in its genome. RNA-seq results revealed that *adhE1* was transcribed at a significantly higher level than *adhE2* (see below), indicating that AdhE1 is the dominant functional enzyme involved in the conversion of acetaldehyde to ethanol. This is in agreement with the result for the AdhE activity assay, in which *adhE1* deletion resulted in significantly decreased AdhE enzyme activity in cell extract (Table 1). Regarding ethanol synthesis, *adhE1* deletion did not eliminate ethanol production, which is consistent with previous results (30). AOR activity (specific activity, 0.01 U/mg) was detected in the cell extract of the $\Delta adhE1$ strain, suggesting that some acetaldehyde was generated. We speculated that acetaldehyde can be reduced by AdhE2 or other alcohol dehydrogenases, resulting in ethanol production. Interestingly, the $\Delta adhE1$ strain produced more ethanol than the WT under the same fermentation conditions in this study. This phenotype was also observed during fermentation by the $\Delta adhE1$ mutant of *C. autoethanogenum* on CO, which produced 171% to 183% higher titers of ethanol than the WT (15). Why the $\Delta adhE1$ strain produced markedly higher levels of ethanol remains an enigma.

Because of the inactivation of both *adhE* genes, the $\Delta adhE1 \Delta adhE2$ mutant strain must use other metabolic pathways to recycle reducing equivalents. YTF medium

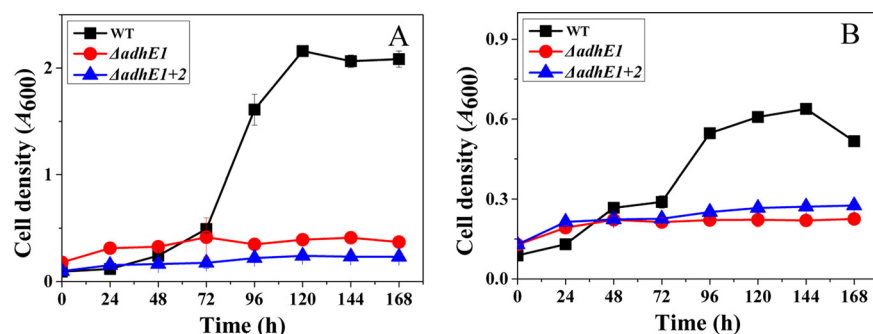


FIG 3 Growth profiles of *C. ljungdahlii* WT (black squares), $\Delta adhE1$ mutant (red circles), and $\Delta adhE1 \Delta adhE2$ mutant (blue triangles) strains on syngas. (A) CO:CO₂ (80:20, vol/vol). (B) H₂:CO₂ (60:40, vol/vol).

contains 10 g/liter yeast extract and 16 g/liter tryptone, which can supply the required metabolites for fermentation by *C. ljungdahlii*. Then, reducing equivalents can be recycled through biochemical reactions, in which these metabolites participate. Therefore, the $\Delta adhE1 \Delta adhE2$ mutant strain grew well in YTF medium. In contrast, *C. ljungdahlii*, to a large extent, depends on ADHs to achieve NADH reoxidation in modified DSMZ 879 medium. Thus, the $\Delta adhE1 \Delta adhE2$ mutant strain displayed significant growth deficiency and lost its capacity for ethanol production in modified DSMZ 879 medium.

Batch fermentation of *adhE* deletion mutants on syngas. In the case of gas fermentation with CO or H₂:CO₂ as the carbon and energy sources, the $\Delta adhE1$ and $\Delta adhE1 \Delta adhE2$ mutants exhibited significantly diminished growth and an inability to generate ethanol (Fig. 3). The WT grew well on CO and achieved a much higher cell density (A_{600} , 2.1 ± 0.1) than the mutants (0.4 ± 0.02 for the $\Delta adhE1$ mutant and 0.24 ± 0.02 for the $\Delta adhE1 \Delta adhE2$ mutant). In addition, 28 ± 5 mM ethanol was detected in the end products in the WT. The fermentation profiles of the WT and mutants grown on H₂:CO₂ were similar to those grown on CO (Table 2; Fig. S4 and S5). Analysis of syngas uptake indicated that the WT consumed more syngas than the *adhE* deletion mutants. Taken together, these results demonstrated that AdhE plays a critical role in growth and metabolism during gas fermentation by *C. ljungdahlii*.

Fed-batch fermentation of WT under controlled pH and gas pressure. To provide a preferable growth condition for the WT, the fermentation process was controlled at pH 6.0 and at a pressure of 0.1 MPa with a constant CO:CO₂ supply (vol/vol, 80/20). *C. ljungdahlii* exhibited excellent growth, and the density of cell growth reached an A_{600} of 2.2 ± 0.2 . The end products included 177 ± 0.8 mM acetate, 24 ± 0.5 mM 2,3-butanediol, and trace amounts of lactate. Interestingly, the ethanol concentration (107 ± 0.6 mM) peaked at 84 h in the course of batch fermentation (Fig. 4). Analysis of ethanol synthesis and cell growth indicated that ethanol was largely produced during the exponential phase and oxidized during the stationary phase, which was also observed in previous studies (13, 15).

TABLE 2 Headspace pressure change and the final product titers of *C. ljungdahlii* WT, $\Delta adhE1$ mutant, and $\Delta adhE1 \Delta adhE2$ mutant on syngas

Strain	CO:CO ₂ (vol/vol, 80/20)		CO ₂ :H ₂ (vol/vol, 40/60)		CO:CO ₂ (vol/vol, 80/20)		CO ₂ :H ₂ (vol/vol, 40/60)	
	Ethanol (mM)	Acetate (mM)	Ethanol (mM)	Acetate (mM)	SP ^b (MPa)	CO:CO ₂ (vol/vol)	SP (MPa)	CO ₂ :H ₂ (vol/vol)
Wild type	28 ± 5	53 ± 5	10 ± 2	61 ± 2	0.06 ± 0.02	1:9	0.08 ± 0.02	3:4
$\Delta adhE1$ mutant	ND ^a	19 ± 0.3	ND	13 ± 2	0.13 ± 0.04	1:1	0.11 ± 0.04	4:5
$\Delta adhE1 \Delta adhE2$ mutant	ND	15 ± 0.5	ND	20 ± 1	0.14 ± 0.03	1:1	0.11 ± 0.01	1:1

^aND, not detectable.

^bSP, space pressure. The beginning space pressure is 0.2 MPa.

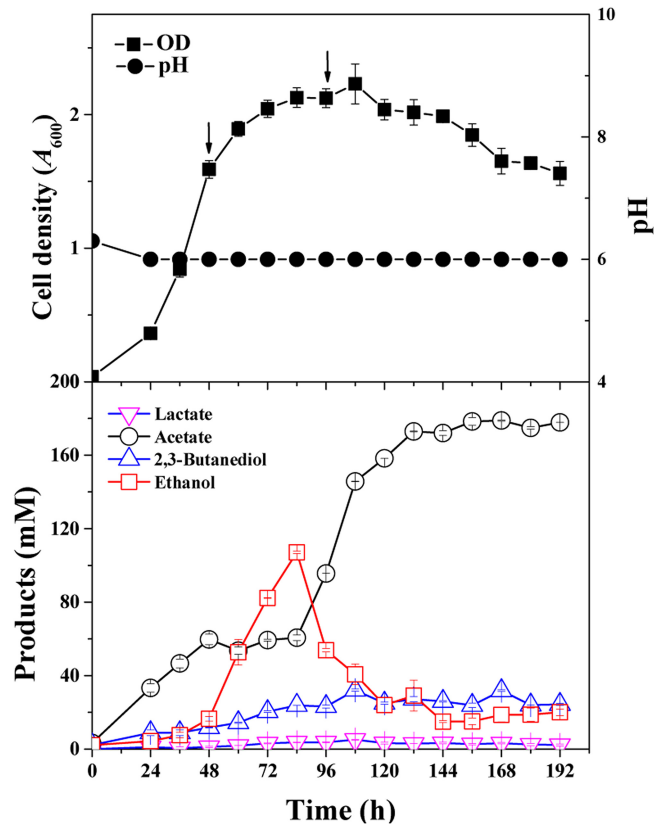


FIG 4 Growth and product concentrations of *C. ljungdahliae* WT grown on CO:CO₂ (vol/vol, 80/20) with pH 6.0 and gas pressure of 0.1 MPa. Arrows: these two time points represent the exponential and stationary growth phases, respectively. Samples were taken out of the bioreactor at these time points for ethanol oxidation and RNA-Seq analysis.

ATP is the universal energy equivalent in microbial growth, and demand for ATP is high during the exponential phase, in which biomass is quickly accumulated. During gas fermentation by *C. ljungdahliae*, NADH is produced as an electron carrier in large quantities, accompanied by ATP synthesis (13, 21). We hypothesized that ethanol was a preferred product as an additional NADH sink to maintain the redox balance during gas fermentation. During the stationary phase, biomass no longer accumulates, and less ATP and NADH are produced. However, NADH is still needed. Thus, ethanol oxidation occurs at this stage to provide energy and reducing equivalents to fulfill the survival of cells. The fed-batch fermentation result in this study supports our hypothesis.

Ethanol oxidation in CO fermentation. Gas chromatography-mass spectrometry (GC-MS) was used to analyze the products of ethanol oxidation using ¹³C-labeled ethanol and acetate, which have higher mass weights than unlabeled molecules. In a mixture containing stationary cells collected at 96 h and ¹³C-labeled acetic acid, only a trace amount of ¹³C-labeled ethanol was detected up to 12 h (Fig. 5 and Fig. S6). On the other hand, with the addition of ¹³C-labeled ethanol, a large amount of ¹³C-labeled acetic acid was detected. These results suggest that ethanol could be used by *C. ljungdahliae* cells to produce acetate in the absence of CO (no carbon and energy source).

AOR-harboring acetogens, such as *C. ljungdahliae* and *C. autoethanogenum*, are capable of reducing acetate to ethanol during gas fermentation. According to our work and some published results, alcohols, including ethanol and butanol, could also be converted into their corresponding primary carboxylic acids (13, 15). These results suggest the existence of a flexible metabolic mechanism that regulates the conversion between ethanol and acetate. The redox reaction of acetate to acetaldehyde with Fd_{red}

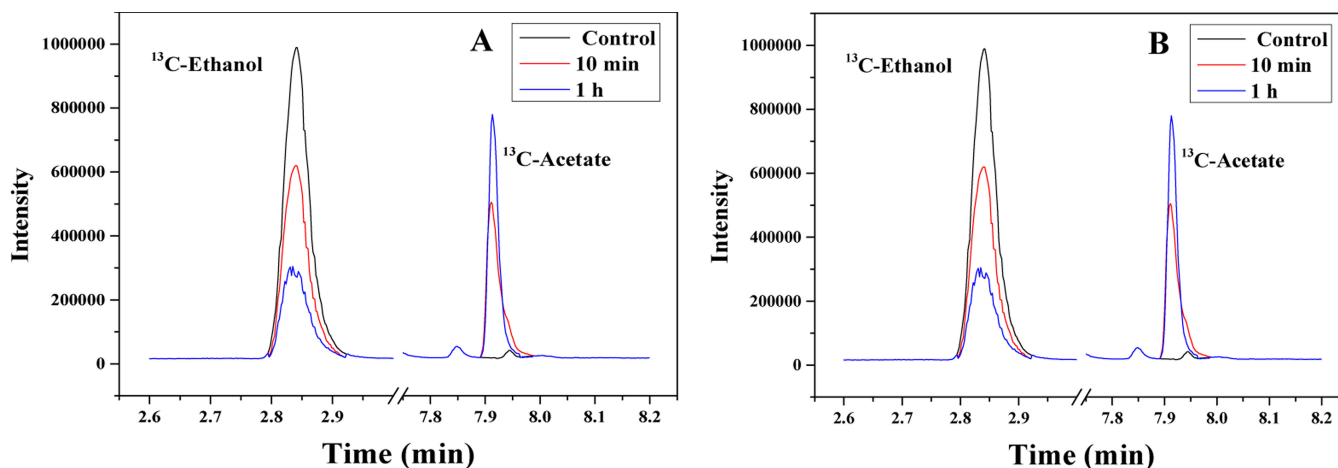


FIG 5 Detection of ^{13}C labeled products after incubation of *C. ljungdahlii* WT cells in fresh medium with ^{13}C -acetate (A) or ^{13}C -ethanol (B) under anaerobic conditions.

is thermodynamically unfavorable under standard conditions ($\Delta G^{\circ} = 35 \text{ kJ/mol}$). However, this reaction can occur under physiological conditions with an intracellular pH of 6.0 and 1,000-fold higher intracellular acetate levels versus acetaldehyde (31). During gas fermentation by *C. ljungdahlii*, CO, as a carbon and energy source, is metabolized quickly for growth during the exponential phase (6, 32). Under this condition, Fd_{red} , ATP, NADPH, and NADH can be quickly produced (Fig. 1). Acetate can be converted to ethanol through the AOR pathway for recycling of reducing equivalents to maintain the redox balance during metabolism. During the stationary phase, biomass production ceases, resulting in a reduction of ATP demand. Therefore, the oxidation of ethanol to acetate is driven by a thermodynamic balance, during which reducing equivalents are released. It is noted that no ATP was produced during ethanol oxidation. This speculation can explain why ethanol production increased during the exponential phase and decreased during the stationary phase (17, 18, 33). Chemostat technology can maintain a constant growth of strains at a specific dilution rate with pH control in the bioreactor. Under optimal conditions, biomass and ethanol are produced in large quantities, and ethanol oxidation does not occur (33).

The pathway of ethanol oxidation. Ethanol can be biosynthesized through both the AdhE and AOR pathways (Fig. 1). Which pathway is used by *C. ljungdahlii* during ethanol oxidation? Though acetate and ethanol have identical stoichiometry regarding carbon balance as C2-compounds in end products, their energy metabolism is significantly different between the AdhE and AOR pathways during gas fermentation. Through the AdhE pathway, 2 mol of NADH and 1 mol of ATP are produced during ethanol oxidation to acetate, whereas through the AOR pathway, 1 mol of Fd_{red} and 1 mol of NADH are produced. During CO fermentation, NADPH is formed by electron bifurcation of Fd_{red} and NADH via Fd-dependent transhydrogenase (Nfn) (18). Therefore, the NAD^+/NADH and $\text{NADP}^+/\text{NADPH}$ ratios were determined to figure out the pathway for ethanol oxidation to acetate (Fig. 6). It was found that the NAD^+/NADH ratio increased during the exponential phase and decreased during the stationary phase, which was consistent with the ethanol titer profile in the broth, indicating that ethanol synthesis requires electron transfer from NADH and ethanol oxidation supplies electrons to NAD^+ . Furthermore, the $\text{NADP}^+/\text{NADPH}$ ratio curve was identical to the NAD^+/NADH ratio curve throughout fermentation (Fig. 6B), revealing that the $\text{Fd}_{\text{ox}}/\text{Fd}_{\text{red}}$ ratio varied during ethanol oxidation. Therefore, our results indicated that ethanol is oxidized by the AOR pathway. This means ethanol generation and reuse share the same metabolic pathway during gas fermentation in *C. ljungdahlii*. Our observation provides evidence explaining why deletion of *aor2* or *adhE1* enhances the production of ethanol in *C. autoethanogenum* fermentation (15). Inactivation of *aor2* or *adhE1* blocks ethanol oxidation, thereby increasing the titers of ethanol in the broth.

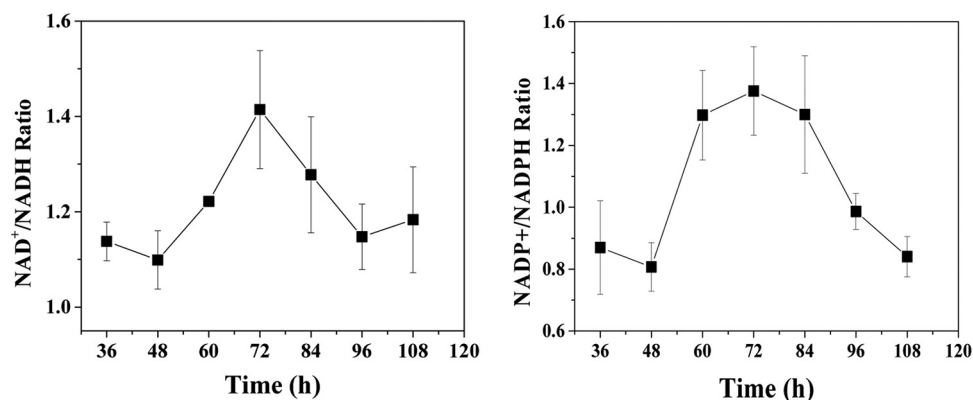


FIG 6 Time courses of NAD⁺/NADH and NADP⁺/NADPH ratios during fermentation in *C. ljungdahlii* WT grown on CO:CO₂ (vol/vol, 80/20).

Transcriptional analysis of ethanol biosynthesis and oxidation. Because of ethanol production and oxidation, carbon and redox flows were distinctly different at the exponential (48 h) and stationary (96 h) phases. Comparative transcriptomics was performed using RNA-Seq technology to investigate intracellular flux patterns at the transcriptional level. Table S2 lists 49 genes involved in the central carbon and energy metabolic pathways. As speculated, *C. ljungdahlii* required ATP for biomass production; thus, the genes related to ATP formation, which include Rnf-ATPase system genes, AdhE pathway genes, acetate formation genes, and the Nfn gene, had higher transcriptional levels in the exponential phase than in the stationary phase. Although the WLP is an ATP-consuming pathway during formyl-THF formation, it is the sole CO fixation pathway and principal metabolic pathway involved in gas fermentation. Therefore, the expression levels of genes involved in the WLP are higher during the exponential phase. During the stationary phase, biomass production ceases, and the efficiency of carbon source uptake is decreased (Fig. 7).

The comparative transcriptomics results suggest that the expression levels of *aor2* and CO dehydrogenase complex genes participating in central metabolic pathways are higher during the stationary phase. This result further proves that the AOR pathway plays a critical role in ethanol oxidation. Based on gene function analysis, both pathways are responsible for important ferredoxin-dependent redox reactions. Fd_{red} is the original energy source for CO fermentation. Genes related to Fd_{red} formation are highly expressed, indicating that *C. ljungdahlii* requires energy for metabolism during the stationary phase. However, detailed functions of this CO dehydrogenase remain to be further studied beyond the transcriptional level. Notably, during H₂:CO₂ fermentation, primary energy is derived from the electron bifurcation reaction of the hydrogenase complex rather than from CO reduction during gas fermentation by *C. ljungdahlii*, and ethanol is also oxidized during H₂:CO₂ fermentation in *C. autoethanogenum* (15). Stoichiometric analysis of ATP gains based on gas fermentation by *C. ljungdahlii* revealed that the ATP yield is 0.75 mol ATP with 1 mol of acetate formed during autotrophic growth on H₂:CO₂, in contrast to 10 mol of ATP with 1 mol of acetate, 1 mol of 2,3-butanediol, and 4 mol of ethanol formed for cells grown on CO (34).

Formate dehydrogenases (FDHs) catalyze the first step in the carbonyl branch of the WLP. Interestingly, all genes related to the WLP are organized in a huge gene cluster (Clju_c37550 to -37670). *fdh* genes are not located in this cluster, and some are located distant from this cluster in the chromosome (13). The genome of *C. ljungdahlii* contains three gene clusters that encode potential FDHs. At the transcriptional level, the *fdh* gene expression level indicated by the reads per kilobase per million (RPKM) value is high. However, the fold change values are not greater than 2. We consider that their transcription profiles during the exponential and stationary phases do not significantly change. Furthermore, FDH forms a complex with an electron-bifurcating hydrogenase,

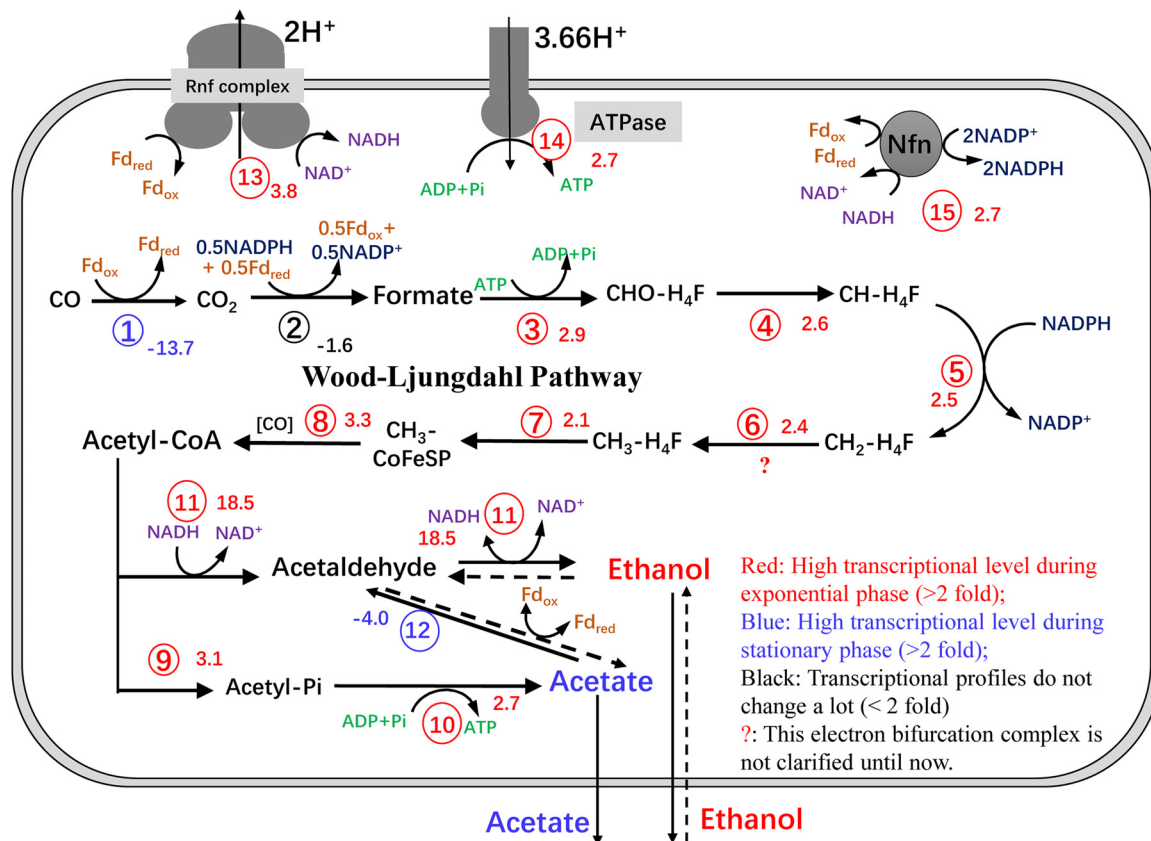


FIG 7 Schematic of the central metabolic pathways of *C. ljungdahlii* grown on CO:CO₂ (vol/vol, 80/20). The sequence numbers represent the correlation enzyme or enzyme complex participating in the metabolic reactions listed in detail in Table S2. The positive values represent the increased change fold during the exponential phase. The negative values represent the decreased change fold during the exponential phase.

and this complex accounts for 6% (m/m) of all cytoplasmic proteins involved in *C. autoethanogenum* growth on CO (18). These results suggest that FDHs play an important role in the metabolic processes of gas fermentation during both the exponential and stationary phases.

The expression profiles of nine genes related to central metabolic pathways were investigated during the exponential and stationary phases via quantitative real-time PCR to verify the RNA-Seq result (Fig. S7). The results indicated that the fold change trends of these key genes were consistent with the findings of RNA-Seq analysis.

Conclusions. The Rnf-ATPase system plays a critical role in NADH production, accompanied by ATP generation during gas fermentation by *C. ljungdahlii* (4, 11, 35, 36). Ethanol synthesis is a preferred strategy for recycling NADH/NAD⁺ to maintain the redox balance during autotrophic growth. Therefore, deletion of both *adhE* genes leads to significant growth deficiencies. In this study, an ethanol oxidation phenotype was clearly observed during fed-batch fermentation with pH and gas pressure control. Combined with the results of key gene knockout, we propose that ethanol synthesis and oxidation are closely related to the growth phase during gas fermentation. Ethanol is synthesized as an NADH sink to achieve redox balance during the exponential phase and is oxidized during the stationary phase in the classic batch fermentation of *C. ljungdahlii*. These findings provide experimental proof to explain some important previously divulged results. (i) Why does the *aor2* deletion mutant of *C. autoethanogenum* produce up to 2.5-fold more ethanol than the WT strain under the same growth condition (15)? Our results indicate that AOR2, as well as AdhE1, is responsible for ethanol oxidation during the stationary phase. Inactivation of *aor2* blocks the oxidation pathway, resulting in a high ethanol concentration in end products. (ii) Why is contin-

TABLE 3 Primers used in this study

Name	Sequence (5'–3')
adhE2gRNAs	AATCTTAAGGAGGAGTTTTCGTCGACGACGAAGCACTCCTAAAGGCGTTTTAGAGCTAG
gRNAaster	ATAAAAATAAGAAGCCTGCAATGCAGGCTTCTTATTTTTATAAAAAAAGCACCGACTC
adhE2uas	TTGCAGGCTTCTTATTTTTATATATTGGAAAGTTGGTAAAGGATATATGGTAG
adhE2us	TTTATTTTTCTTCTTGTCTTCTTCCACAGTCATTAATTAACGACACCTCTTCC
adhE2das	ACTGTGGAGAAGAAAACAAGAAAGAAAAATAAATATATAATAAATTG
adhE2ds	AAGCTTGCATGTCTGCAGGCTCGAGCACCATGCCTCTGGCTTAGATCCCCTAAAAG
adhE1-f	AAGGATATATGGTAGTATTGCAGG
adhE2-r	GCTCAATTTTATTACTGCAGTCAC

uous fermentation (chemostat fermentation) suitable for ethanol production using syngas as a feedstock in *C. autoethanogenum* and *C. ljungdahlii* (17, 18, 33)? Our study results illustrated that biomass production is a prerequisite for ethanol production. Continuous fermentation technology maintains strain growth at a constant rate, and ATP is continuously produced. This prompts continuous ethanol biosynthesis rather than oxidation.

MATERIALS AND METHODS

Bacterial strains and media. *Escherichia coli* strains were cultivated at 37°C in LB medium in the presence of appropriate antibiotics for general plasmid propagation and cloning. *C. ljungdahlii* DSM 13528 was purchased from the Deutsche Sammlung von Mikroorganismen und Zellkulturen GmbH, Braunschweig, Germany, and conserved by freezing mid-exponential phase cultures at –80°C with 20% glycerol. The cultures were cultivated at 37°C under anaerobic conditions. YTF medium was used in mutant construction, and a modified DSMZ 879 medium with a headspace of a gas mixture (CO:CO₂, 80:20 or H₂:CO₂, 60:40) as the carbon source was used in gas fermentation (35, 37). The modified DSMZ 879 medium has the following composition (per liter): 1.0 g NH₄Cl, 0.1 g KCl, 0.2 g MgSO₄·7H₂O, 0.8 g NaCl, 0.02 g CaCl₂·2H₂O, 0.1 g KH₂PO₄, 2.5 mg Na₂WO₄·2H₂O, 1.0 g NaHCO₃, 1.0 g cysteine-HCl·H₂O, 1 g yeast extract, 0.5 g cysteine, 0.5 mg resazurin, 10 ml trace element solution, and 10 ml vitamin solution. Trace element solution contains 2.0 g nitrilotriacetic acid, 1.3 g MnCl₂·H₂O, 0.4 g FeSO₄·7H₂O, 0.2 g CoCl₂·7H₂O, 0.2 g ZnSO₄·7H₂O, 0.2 g Na₂MoO₄·2H₂O, 0.02 g NiCl₂·6H₂O, and 0.1 g Na₂SeO₃·5H₂O in 1 liter distilled water. The vitamin solution contains 2 mg biotin, 2 mg folic acid, 10 mg pyridoxine-HCl, 25 mg thiamine-HCl·2H₂O, 5 mg riboflavin, 5 mg nicotinic acid, 5 mg D-Ca-pantothenate, 0.1 mg vitamin B₁₂, 5 mg *p*-aminobenzoic acid, and 5 mg lipoic acid in 1 liter distilled water. Analytical-grade chemicals used in the medium were purchased from Sinopharm Chemical Reagent Co., Ltd. (Shanghai, China). All antibiotics were purchased from Sangon Co., Ltd. (Shanghai, China).

Plasmid construction and $\Delta adhE1 \Delta adhE2$ mutant deletion. Using the *adhE1*-deleted *C. ljungdahlii* strain as the parent (30), we deleted the *adhE2* gene, yielding a $\Delta adhE1 \Delta adhE2$ mutant. The strains and primers used in this study are listed in Tables 3 and 4. The CRISPR/Cas9 editing plasmid, pMTCas-adhE2, was constructed for *adhE2* deletion in *C. ljungdahlii*. The plasmid pMTCas-adhE1 was digested with Sall/XhoI, yielding a linear vector without the original single guide RNA (sgRNA) and two homologous arms (HAs). The sgRNA that targets the 20-nucleotide (nt) target spacer of *adhE2* was obtained by PCR-amplification using the primers adhE2gRNAs/gRNAaster with pMTCas-adhE1 as the template. The two HAs that flank the coding region of *adhE2* were PCR-amplified from *C. ljungdahlii* genomic DNA using the primers adhE2uas/adhE2us and adhE2ds/adhE2das. Then, the fragments of sgRNA and HAs were assembled through an overlap extension PCR, yielding the sgRNA-HA fragment. Finally, the above-mentioned linear vector (derived from pMTCas-adhE1) and sgRNA-HA fragment were assembled using the ClonExpress MultiS one-step cloning kit (Vazyme Biotech Co. Ltd., Nanjing, China), which resulted in the target plasmid pMTCas-adhE2.

TABLE 4 Strains and plasmids used in this study

Strain or plasmid name	Characteristics	Reference or source
Strains		
<i>C. autoethanogenum</i> DSM 10061 (wild type)		DSMZ
<i>C. ljungdahlii</i> DSM 13528 (wild type)		DSMZ
$\Delta adhE1$ mutant	DSM 13528 $\Delta adhE1$	30
$\Delta adhE1 \Delta adhE2$ mutant	DSM 13528 $\Delta adhE1 \Delta adhE2$	This work
Plasmids		
pMTCas-adhE1	pCB102 <i>ori</i> , <i>catP</i> , ColE1, <i>tra</i> , PthI-Cas9, ParaE-sgRNA, <i>adhE1</i> homologous arm	30
pMTCas-adhE2	pCB102 <i>ori</i> , <i>catP</i> , ColE1, <i>tra</i> , PthI-Cas9, ParaE-sgRNA, <i>adhE2</i> homologous arm	This work

Then, the target plasmid was transferred into *adhE1*-deleted *C. ljungdahlii* by electroporation to delete *adhE2* according to the protocol (30). The *C. ljungdahlii* mutant containing deletions in both *adhE1* and *adhE2* was named the $\Delta adhE1 \Delta adhE2$ mutant.

Batch fermentation with gas. Batch fermentation was performed in a 250-ml screw-cap bottle with a 50-ml working volume in triplicate. The medium was assembled in a Coy anaerobic chamber (Grass Lake, MI, USA). After autoclaving, FeSO_4 , vitamins, cysteine-HCl, and NaHCO_3 were added using syringes with a 0.2- μm filter. Then, gases in the headspace were substituted by $\text{CO}:\text{CO}_2$ (80:20, vol/vol) or $\text{H}_2:\text{CO}_2$ (60:40, vol/vol) as required with a pressure of 0.2 MPa every 12 h. Fed-batch fermentation was carried out in a FUS-5L bioreactor (Gouqiang Biotech Co. Ltd., Shanghai, China) containing 2.5 liters of modified DSM 879 medium. The gases were controlled at a constant pressure of 0.1 MPa. The stirring rate was 250 rpm, and the pH was maintained at 6.0 automatically by adding 2 M KOH. A 300-ml preculture of *C. ljungdahlii* was inoculated into the bioreactor, and 5-ml samples were withdrawn every 12 h for cell density monitoring and product analysis.

Preparation of cell extracts and enzyme activity analysis. Wild-type, $\Delta adhE1$ mutant, and $\Delta adhE1 \Delta adhE2$ mutant strains were cultured in YTF medium with 5 g/liter fructose until the late-exponential phase. Cells were collected by centrifugation at $10,000 \times g$ at 4°C under strictly anoxic conditions and were resuspended in 20 ml of anoxic 50-mM potassium phosphate (pH 7.4) containing 2 mM dithiothreitol (DTT). Lysozyme was added to the cell suspension, and the mixture was incubated at 37°C for 30 min. Then, it was moved to an anaerobic chamber for ultrasonication. Finally, cells debris was removed by centrifugation at $35,000 \times g$ at 4°C for 1 h. The protein concentration was determined using the Bradford method (18).

Acetaldehyde:ferredoxin oxidoreductase activity and ethanol dehydrogenase activity were determined under strictly anoxic conditions at 37°C in 1.5-ml anaerobic cuvettes sealed with rubber stoppers (Hellma GmbH, Müllheim, Germany). The cuvettes were filled with pure N_2 at 1.2×10^5 Pa as the gas phase before use to maintain anaerobic conditions during enzyme catalysis. The reactions were monitored photometrically at the specified wavelength. Ferredoxin reduction was monitored at 430 nm ($\Delta \epsilon_{\text{ox-red}} \approx 13.1 \text{ mM}^{-1} \text{ cm}^{-1}$), and NADH formation was monitored at 340 nm ($\Delta \epsilon_{\text{ox-red}} \approx 6.2 \text{ mM}^{-1} \text{ cm}^{-1}$). One unit (1 U) was defined as the transfer of 2 μmol electrons min^{-1} . For the acetaldehyde:ferredoxin oxidoreductase activity assay, the mixture contained 50 mM Tris-HCl (pH 7.4), 2 mM DTT, 1.5 mM acetaldehyde, and 30 μM ferredoxin. For alcohol dehydrogenase activity determination, the assay mixture contained 50 mM Tris-HCl (pH 7.4), 2 mM DTT, 1.5 mM ethanol, and 1 mM NAD^+ (17, 18).

Ferredoxin was obtained by heterologous expression of gene WP_013236834.1 from *C. autoethanogenum* in *E. coli* C41 (38–40). Gene amplification was performed by PCR with genomic DNA of *C. autoethanogenum* as the template. The following primers were used: 5'-CATGCCATGGCATATAAAATTA CAGAGGAT-3' (reverse primer, the NcoI restriction site is underlined); 5'-CCGCTCGAGGCTTTCTCAACT GGTGCTC-3' (forward primer, the XhoI restriction site is underlined). The PCR fragment was digested by restriction endonucleases and subsequently ligated into expression vector pET28b, which had been digested by the same restriction endonucleases. Finally, the constructed plasmid was transferred into *E. coli* C41 (DE3), which already harbored plasmids pRKISC and pCodonPlus for production of iron-sulfur proteins. Cell cultivation and ferredoxin purification steps were performed as previously described (38). Ferredoxin was stored at -20°C in an N_2 atmosphere until use.

Gene expression analysis by RNA-Seq. Comparative transcriptomics of cells between the exponential and stationary phases was performed to investigate gene expression profiles based on two biological replicates. Cell pellets cultured in a bioreactor were collected by centrifugation at $10,000 \times g$ at -4°C for 48 h and 96 h and then were immediately frozen in liquid nitrogen and stored at -80°C . RNA isolation and high-throughput RNA sequencing (RNA-Seq) were conducted by Oebiotech Corp. (Shanghai, China). Total RNA was extracted using a mirVana microRNA (miRNA) isolation kit (Ambion, Santa Clara, CA, USA) following the manufacturer's protocol. RNA integrity was evaluated using an Agilent 2100 bioanalyzer (Agilent Technologies, Santa Clara, CA, USA). Samples with an RNA integrity number (RIN) of ≥ 7 were subjected to subsequent analysis. Libraries were constructed using a TruSeq stranded mRNA LTSample prep kit (Illumina, San Diego, CA, USA) according to the manufacturer's instructions. Then, these libraries were sequenced on an Illumina sequencing platform (HiSeq 2500), and 150-bp/125-bp paired-end reads were generated. Based on reads per kilobase of transcript per million mapped reads (RPKM) normalization, the gene expression profiles were analyzed.

In order to confirm the authenticity of RNA-Seq data, the expressions of nine key genes located in the central metabolic pathway were evaluated using quantitative real-time PCR (qRT-PCR) on a Light-Cycler 480 system (Roche Applied Science, Indianapolis, USA) (35). cDNA synthesis was performed according to the instructions from TransGen Biotech Co., Beijing, China. The genes and primers used here are shown in Table S1. All quantitative PCRs were repeated in three biological and three technical replications.

Analytical method. Cell growth was determined spectrophotometrically at 600 nm (A_{600}) using a UV/visible Ultrospec 2100 Pro spectrophotometer (GE Healthcare, USA). The concentrations of fructose, ethanol, acetic acid, lactate, and 2,3-butanediol were determined using an Agilent 1100 high-performance liquid chromatography (HPLC) system with an Agilent Hi-Plex H column equipped with a refractive index detector and operated at 35°C . Column temperature was maintained at 55°C . Slightly acidified (5 mM H_2SO_4) water was used as the mobile phase at a flow rate of 0.7 ml/min. Molecular hydrogen (H_2) and carbon dioxide (CO_2) were detected using a gas chromatography device (GC-7820; Lunan Analysis Instruments Co. Ltd., Tengzhou, China) equipped with a TDX-01 column (2-m length, 3-mm inner diameter). The gas mixture was determined by a thermal conductivity detector with

high-purity argon acting as the carrier gas. Changes in the headspace pressure of bottles during gas fermentation were measured using a Hakin pressure detector (Hakin Instruments Co. Ltd., Qingdao, China).

A GC-mass spectrometry (GC-MS) system (Agilent 7890AGC) with a 5,975 C mass selective detector was used to analyze ^{13}C -labeled ethanol and acetate. A 30-m HP-INNOWax column with a 0.25 mm inner diameter and 0.25 μm thickness was used, and helium was the carrier gas at 1 ml/min. The MS instrument was operated in the full scan mode to detect ethanol and acetate. One μl of sample was injected with the injection port temperature at 250°C. The temperature program was as follows: 50°C at 2 min, then increasing 10°C/min to 70°C and 25°C/min to 250°C, and then 250°C for 14 min. ^{13}C -labeled ethanol or acetate was added into the modified DSM 879 medium to achieve a final concentration of 1 g/liter and was analyzed with a mass spectrometer (InertXL MSD; Agilent Technologies). The cells growing in CO under controlled pH and gas pressure were taken out of the bioreactor at the exponential and stationary phases. Cells were collected by centrifugation at $7,500 \times g$ for 5 min at room temperature under anaerobic conditions. Then, the pellets were resuspended in fresh ^{13}C -labeled ethanol medium and ^{13}C -labeled acetate medium. The tubes were incubated at 37°C, and the reaction was stopped at different times by cooling on ice and centrifuging at $10,000 \times g$ at 4°C, followed by GC/MS analysis. Carbon atoms in ethanol and acetate were marked by isotope. Thus, the characteristic peak of ^{13}C -labeled acetate and ethanol could be tested by GC-MS to avoid ethanol and acetate in background cells.

The ratios of NADH/NAD⁺ and NADPH/NADP⁺ were measured using Amplitude colorimetric NADH and NADPH assay kits (AAT Bioquest, Inc., Sunnyvale, CA, USA). The cell pellets were washed with 0.1 M ice-cold phosphate-buffered saline (PBS) and then suspended in lysate buffer at room temperature for 15 min prior to analysis. The reaction was carried out in 96-well plates at room temperature for 10 h. The concentrations of NADH, NADPH, NAD⁺, and NADP⁺ were monitored at 460 nm or 635 nm using a microplate reader (BioTek, Winooski, VT, USA).

Data availability. RNA-Seq data were submitted to the ArrayExpress database (www.ebi.ac.uk/arrayexpress) under accession number [E-MTAB-7753](https://www.ebi.ac.uk/arrayexpress/experiments/E-MTAB-7753).

SUPPLEMENTAL MATERIAL

Supplemental material is available online only.

SUPPLEMENTAL FILE 1, PDF file, 0.8 MB.

ACKNOWLEDGMENTS

This study was supported by grants from the National Natural Science Foundation of China (31800026), the Key Laboratory of Biofuel, Chinese Academy of Sciences (CASKLB2018X), QIBEBT Funding (QIBEBT ZZBS 201805), the State Key Laboratory of Microbial Technology Open Projects Fund (M2019-02), the Science and Technology Commission of Shanghai Municipality (17JC1404800), and the China Petrochemical Corporation (Sinopec).

REFERENCES

- Clomburg JM, Crumbley AM, Gonzalez R. 2017. Industrial biomanufacturing: the future of chemical production. *Science* 355: aag0804. <https://doi.org/10.1126/science.aag0804>.
- Liu CG, Xiao Y, Xia XX, Zhao XQ, Peng LC, Srinophakun P, Bai FW. 2019. Cellulosic ethanol production: progress, challenges and strategies for solutions. *Biotechnol Adv* 37:491–504. <https://doi.org/10.1016/j.biotechadv.2019.03.002>.
- Molitor B, Richter H, Martin ME, Jensen RO, Juminaga A, Mihalcea C, Angenent LT. 2016. Carbon recovery by fermentation of CO-rich off gases: turning steel mills into biorefineries. *Bioresour Technol* 215: 386–396. <https://doi.org/10.1016/j.biortech.2016.03.094>.
- Marcellin E, Behrendorff JB, Nagaraju S, DeTissera S, Segovia S, Palfreyman RW, Daniell J, Licona-Cassani C, Quek LE, Speight R, Hodson MP, Simpson SD, Mitchell WP, Köpke M, Nielsen LK. 2016. Low carbon fuels and commodity chemicals from waste gases: systematic approach to understand energy metabolism in a model acetogen. *Green Chem* 18:3020–3028. <https://doi.org/10.1039/C5GC02708J>.
- Liew F, Martin ME, Tappel RC, Heijstra BD, Mihalcea C, Köpke M. 2016. Gas fermentation: a flexible platform for commercial scale production of low-carbon-fuels and chemicals from waste and renewable feedstocks. *Front Microbiol* 7:694. <https://doi.org/10.3389/fmicb.2016.00694>.
- Liew F, Henstra AM, Winzer K, Köpke M, Simpson SD, Minton NP. 2016. Insights into CO₂ fixation pathway of *Clostridium autoethanogenum* by targeted mutagenesis. *mBio* 7:e00427-16. <https://doi.org/10.1128/mBio.00427-16>.
- Dürre P, Eikmanns BJ. 2015. C1-carbon sources for chemical and fuel production by microbial gas fermentation. *Curr Opin Biotechnol* 35: 63–72. <https://doi.org/10.1016/j.copbio.2015.03.008>.
- Adamberg K, Valgepea K, Vilu R. 2015. Advanced continuous cultivation methods for systems microbiology. *Microbiology* 161:1707–1719. <https://doi.org/10.1099/mic.0.000146>.
- Munasinghe PC, Khanal SK. 2012. Syngas fermentation to biofuel: evaluation of carbon monoxide mass transfer and analytical modeling using a composite hollow fiber (CHF) membrane bioreactor. *Bioresour Technol* 122:130–136. <https://doi.org/10.1016/j.biortech.2012.03.053>.
- Liu K, Atiyeh HK, Tanner RS, Wilkins MR, Huhnke RL. 2012. Fermentative production of ethanol from syngas using novel moderately alkaliphilic strains of *Alkalibaculum bacchi*. *Bioresour Technol* 104:336–341. <https://doi.org/10.1016/j.biortech.2011.10.054>.
- Köpke M, Mihalcea C, Bromley JC, Simpson SD. 2011. Fermentative production of ethanol from carbon monoxide. *Curr Opin Biotechnol* 22:320–325. <https://doi.org/10.1016/j.copbio.2011.01.005>.
- Munasinghe PC, Khanal SK. 2010. Syngas fermentation to biofuel: evaluation of carbon monoxide mass transfer coefficient ($k_L a$) in different reactor configurations. *Biotechnol Prog* 26:1616–1621. <https://doi.org/10.1002/btpr.473>.
- Köpke M, Held C, Hujer S, Liesegang H, Wiewer A, Wollherr A, Ehrenreich A, Liebl W, Gottschalk G, Durre P. 2010. *Clostridium ljungdahlii* represents a microbial production platform based on syngas. *Proc Natl Acad Sci U S A* 107:13087–13092. <https://doi.org/10.1073/pnas.1004716107>.
- Brown SD, Nagaraju S, Utturkar S, De Tissera S, Segovia S, Mitchell W, Land ML, Dassanayake A, Köpke M. 2014. Comparison of single-molecule se-

- quencing and hybrid approaches for finishing the genome of *Clostridium autoethanogenum* and analysis of CRISPR systems in industrial relevant *Clostridia*. *Biotechnol Biofuels* 7:40. <https://doi.org/10.1186/1754-6834-7-40>.
15. Liew F, Henstra AM, Köpke M, Winzer K, Simpson SD, Minton NP. 2017. Metabolic engineering of *Clostridium autoethanogenum* for selective alcohol production. *Metab Eng* 40:104–114. <https://doi.org/10.1016/j.ymben.2017.01.007>.
 16. Leang C, Ueki T, Nevin KP, Lovley DR. 2013. A genetic system for *Clostridium ljungdahlii*: a chassis for autotrophic production of biocommodities and a model homoacetogen. *Appl Environ Microbiol* 79:1102–1109. <https://doi.org/10.1128/AEM.02891-12>.
 17. Mock J, Zheng YN, Mueller AP, Ly S, Tran L, Segovia S, Nagaraju S, Köpke M, Dürre P, Thauer RK. 2015. Energy conservation associated with ethanol formation from H₂ and CO₂ in *Clostridium autoethanogenum* involving electron bifurcation. *J Bacteriol* 197:2965–2980. <https://doi.org/10.1128/JB.00399-15>.
 18. Wang S, Huang H, Kahnt J, Mueller AP, Köpke M, Thauer RK. 2013. NADP-specific electron-bifurcating [FeFe]-hydrogenase in a functional complex with formate dehydrogenase in *Clostridium autoethanogenum* grown on CO. *J Bacteriol* 195:4373–4386. <https://doi.org/10.1128/JB.00678-13>.
 19. Valgepea K, Loi KQ, Behrendorff JB, Lemgruber RDP, Plan M, Hodson MP, Köpke M, Nielsen LK, Marcellin E. 2017. Arginine deiminase pathway provides ATP and boosts growth of the gas-fermenting acetogen *Clostridium autoethanogenum*. *Metab Eng* 41:202–211. <https://doi.org/10.1016/j.ymben.2017.04.007>.
 20. Valgepea K, de Souza Pinto Lemgruber R, Meaghan K, Palfreyman RW, Abdalla T, Heijstra BD, Behrendorff JB, Tappel R, Köpke M, Simpson SD, Nielsen LK, Marcellin E. 2017. Maintenance of ATP homeostasis triggers metabolic shifts in gas-fermenting acetogens. *Cell Syst* 4:505–515. <https://doi.org/10.1016/j.cels.2017.04.008>.
 21. Schuchmann K, Müller V. 2014. Autotrophy at the thermodynamic limit of life: a model for energy conservation in acetogenic bacteria. *Nat Rev Microbiol* 12:809–821. <https://doi.org/10.1038/nrmicro3365>.
 22. Peters JW, Miller AF, Jones AK, King PW, Adams MWW. 2016. Electron bifurcation. *Curr Opin Chem Biol* 31:146–152. <https://doi.org/10.1016/j.cbpa.2016.03.007>.
 23. Tremblay PL, Zhang T, Dar SA, Leang C, Lovley DR. 2012. The Rnf complex of *Clostridium ljungdahlii* is a proton-translocating ferredoxin: NAD⁺ oxidoreductase essential for autotrophic growth. *mBio* 4:e0040612. <https://doi.org/10.1128/mBio.00406-12>.
 24. Fast AG, Papoutsakis ET. 2012. Stoichiometric and energetic analyses of non-photosynthetic CO₂-fixation pathways to support synthetic biology strategies for production of fuels and chemicals. *Curr Opin Chem Eng* 1:380–395. <https://doi.org/10.1016/j.coche.2012.07.005>.
 25. Fuchs G. 2011. Alternative pathways of carbon dioxide fixation: insights into the early evolution of life? *Annu Rev Microbiol* 65:631–658. <https://doi.org/10.1146/annurev-micro-090110-102801>.
 26. Ragsdale SW, Pierce E. 2008. Acetogenesis and the Wood-Ljungdahl pathway of CO₂ fixation. *Biochim Biophys Acta* 1784:1873–1898. <https://doi.org/10.1016/j.bbapap.2008.08.012>.
 27. Wood HG. 1991. Life with CO or CO₂ and H₂ as a source of carbon and energy. *FASEB J* 5:156–163. <https://doi.org/10.1096/fasebj.5.2.1900793>.
 28. Daniell J, Köpke M, Simpson SD. 2012. Commercial biomass syngas fermentation. *Energies* 5:5372–5417. <https://doi.org/10.3390/en5125372>.
 29. Membrillo-Hernández J, Lin EC. 1999. Regulation of expression of the *adhE* gene, encoding ethanol oxidoreductase in *Escherichia coli*: transcription from a downstream promoter and regulation by *fnr* and *RpoS*. *J Bacteriol* 181:7571–7579. <https://doi.org/10.1128/JB.181.24.7571-7579.1999>.
 30. Huang H, Chai C, Li N, Rowe P, Minton NP, Yang S, Jiang W, Gu Y. 2016. CRISPR/Cas9-based efficient genome editing in *Clostridium ljungdahlii*, an autotrophic gas-fermenting bacterium. *ACS Synth Biol* 5:1355–1361. <https://doi.org/10.1021/acssynbio.6b00044>.
 31. Thauer RK, Jungermann K, Decker K. 1977. Energy conservation in chemotrophic anaerobic bacteria. *Bacteriol Rev* 41:100–180. <https://doi.org/10.1128/MMBR.41.1.100-180.1977>.
 32. Martin ME, Richter H, Saha S, Angenent LT. 2016. Traits of selected *Clostridium* strains for syngas fermentation to ethanol. *Biotechnol Bioeng* 113:531–539. <https://doi.org/10.1002/bit.25827>.
 33. Richter H, Molitor B, Wei H, Chen W, Aristilde L, Angenent LT. 2016. Ethanol production in syngas-fermenting *Clostridium ljungdahlii* is controlled by thermodynamics rather than by enzyme expression. *Energy Environ Sci* 9:2392–2399. <https://doi.org/10.1039/C6EE01108J>.
 34. Zhu HF, Liu ZY, Zhou X, Yi JH, Lun ZM, Wang SN, Tang WZ, Li FL. 2020. Energy conservation and carbon flux distribution during fermentation of CO or H₂/CO₂ by *Clostridium ljungdahlii*. *Front Microbiol* 11:416. <https://doi.org/10.3389/fmicb.2020.00416>.
 35. Xie BT, Liu ZY, Tian L, Li FL, Chen XH. 2015. Physiological response of *Clostridium ljungdahlii* DSM 13528 of ethanol production under different fermentation conditions. *Bioresour Technol* 177:302–307. <https://doi.org/10.1016/j.biortech.2014.11.101>.
 36. Valgepea K, de Souza Pinto Lemgruber R, Abdalla T, Binos S, Takemori N, Takemori A, Tanaka Y, Tappel R, Köpke M, Simpson SD, Nielsen LK, Marcellin E. 2018. H₂ drives metabolic rearrangements in gas-fermenting *Clostridium autoethanogenum*. *Biotechnol Biofuels* 11:55. <https://doi.org/10.1186/s13068-018-1052-9>.
 37. Humphreys CM, McLean S, Schatschneider S, Millat T, Henstra AM, Annan FJ, Breikopf R, Pander B, Piatek P, Rowe P, Wichlacz AT, Woods C, Norman R, Blom J, Goesman A, Hodgman C, Barrett D, Thomas NR, Winzer K, Minton NP. 2015. Whole genome sequence and manual annotation of *Clostridium autoethanogenum*, an industrially relevant bacterium. *BMC Genomics* 16:1085. <https://doi.org/10.1186/s12864-015-2287-5>.
 38. Demmer JK, Huang H, Wang S, Demmer U, Thauer RK, Ermiler U. 2015. Insights into flavin-based electron bifurcation via the NADH-dependent reduced ferredoxin:NADP oxidoreductase structure. *J Biol Chem* 290:21985–21995. <https://doi.org/10.1074/jbc.M115.656520>.
 39. Nakamura M, Saeki K, Takahashi Y. 1999. Hyperproduction of recombinant ferredoxins in *Escherichia coli* by coexpression of the ORF1-ORF2-iscU-iscA-hscB-hscA-fdx-ORF3 gene cluster. *J Biochem* 126:10–18. <https://doi.org/10.1093/oxfordjournals.jbchem.a022409>.
 40. Huang H, Hu L, Yu W, Li H, Tao F, Xie H, Wang S. 2016. Heterologous overproduction of [2Fe4S]- and [2Fe2S]-type clostridial ferredoxins and [2Fe2S]-type agrobacterial ferredoxin. *Protein Expr Purif* 121:1–8. <https://doi.org/10.1016/j.pep.2015.12.019>.